Electronic Supplementary Information (ESI) for Soft Matter

Electronic Supplementary Information (ESI) for Soft Matter:

Master equation for the probability distribution functions of forces in soft particle packings

Kuniyasu Saitoh, Vanessa Magnanimo, and Stefan Luding

Faculty of Engineering Technology, MESA+, University of Twente, Drienerlolaan 5, 7522 NB, Enschede, The Netherlands

In this Electronic Supplementary Information (ESI), we explain some details of system size dependence (Sec. 1), decompression tests (Sec. 2), and the Master equation for the probability distribution functions (PDFs) of overlaps (Sec. 3). We also show some applications of the Master equation (Sec. 4).

1. System size dependence

In this section, we show that the power law scalings of the coefficients in the linear fitting functions (Eq. (3) in the manuscript) and the fluctuations of overlaps around the mean values do not depend on system size. Here, we compare our results of $N = 512, 2048, 8192,$ and 32768 particles. We prepare different 10 samples for some small systems ($N = 512, 2048,$ and 8192) and different 2 samples for the largest one ($N = 32768$) by changing the initial random configurations.

Figure 1 displays double logarithmic plots of the slopes, a_c, offsets, b_n, and standard deviations, v_n ($n = c$ and v), where all the data in $\gamma < 1$ are well described by the power laws,

$$a_c = A_c\gamma^{\alpha_c}, \quad b_n = B_n\gamma^{\beta_n}, \quad v_n = V_n\gamma^{\lambda_n}, \quad (1)$$

respectively, and we do not see their dependence on the system size. The critical amplitudes are given in the manuscript and the exponents are very close to unity, where we find $\alpha_c \cong 1.00, \beta_c \cong 0.96, \beta_v \cong 1.03, \lambda_c \cong 1.00,$ and $\lambda_v \cong 0.95$ in $\gamma < 1$. Here, we neglect highly non-affine regime, $\gamma \geq 1$, where the data start to deviate from the power law scalings, Eq. (1).

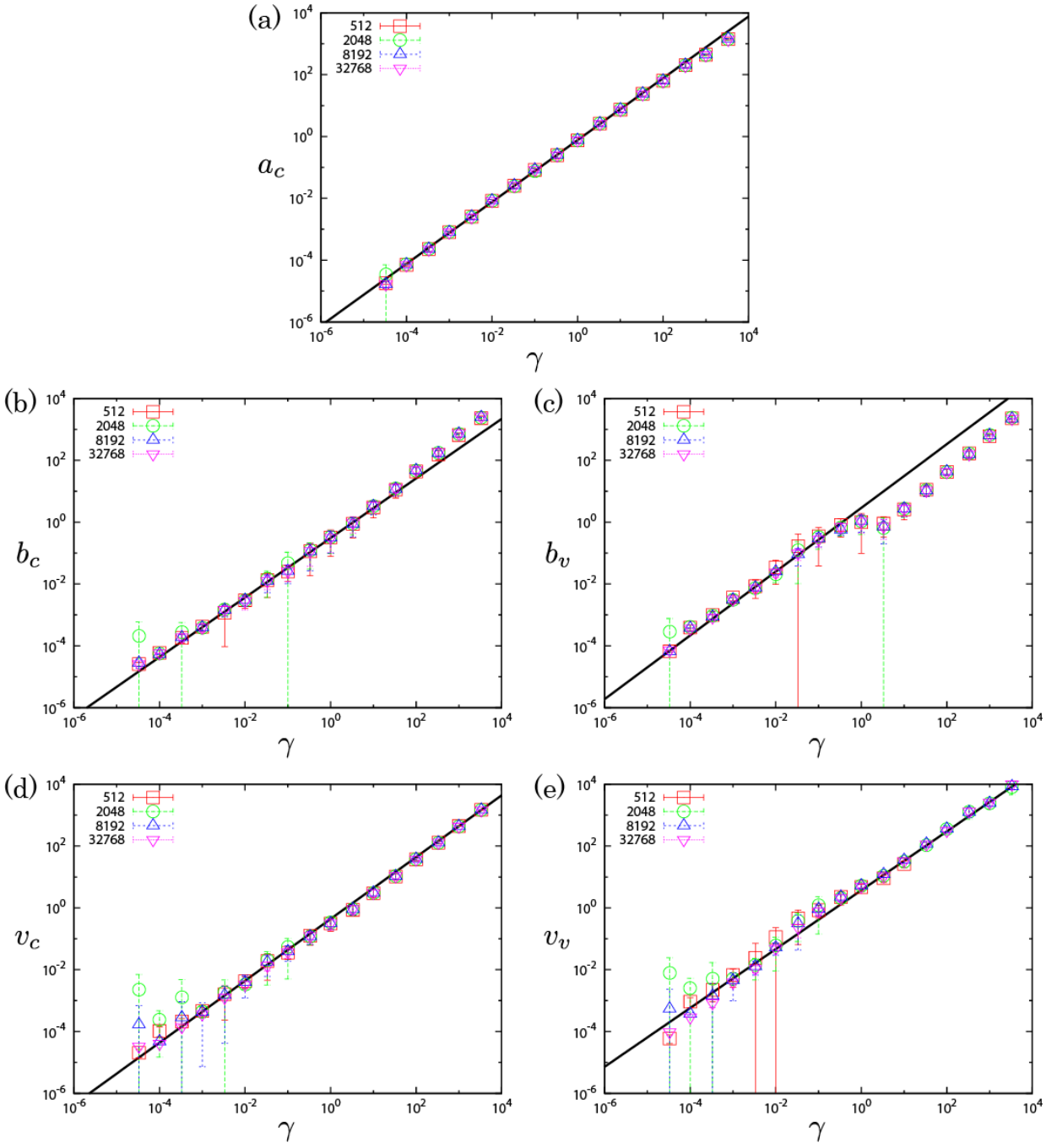

Figure 1. Double logarithmic plots of (a) the slopes in (CC), a_c, (b) offsets in (CC), b_c, (c) offsets in (VV), b_v, (d) fluctuations in (CC), v_c, and (e) fluctuations in (VV), v_v, where different symbols represent different system sizes as listed in the insets. The solid lines are the power law fitting functions, Eq. (1), for $\gamma < 1$.

2. Decompressions

In this section, we explain our additional MD simulations of *decompression* tests, where we decrease the area fraction from ϕ to $\phi + \delta\phi$ ($\delta\phi < 0$) by multiplying every radius by $\sqrt{1 + \delta\phi/\phi}$. Note that we define the increment of area fraction as positive ($\delta\phi > 0$) and negative ($\delta\phi < 0$) for compression and decompression, respectively, so that the scaling parameter is unified to $\gamma \equiv \delta\phi/(\phi - \phi_J)$, i.e. $\gamma > 0$ and $\gamma < 0$ for compression and decompression, respectively.

2-1. Mean and fluctuations

Figure 2 displays double logarithmic plots of the slopes, a_c, offsets, b_n, and fluctuations, v_n ($n = c$ and v), where all the data in $|\gamma| < 1$ are well described by the power laws,

$$a_c = \pm A_c|\gamma|^{\alpha_c},\ \ b_n = \pm B_n|\gamma|^{\beta_n},\ \ v_n = V_n|\gamma|^{\lambda_n}, \quad (2)$$

respectively ($n = c$ and v). Note that the slopes, offsets, and γ are negative for decompressions. Thus, the plus and minus signs in Eq. (2) represent compression and decompression, respectively. Here, we do not show the data in $|\gamma| = \left|\delta\phi/(\phi - \phi_J)\right| \geq 1$ for decompressions, because "unjamming transitions" happen if $|\delta\phi|$ exceeds the distance from jamming before decompression, $\phi - \phi_J$. In Eq. (2), the amplitudes and exponents are the same as in Eq. (1). Therefore, if we roughly estimate the exponents as 1, the coefficients are simply represented as $a_c \sim \gamma$, $b_n \sim \gamma$, and $v_n \sim |\gamma|$ for both compression ($\gamma > 0$) and decompression ($\gamma < 0$). Here, we also neglect highly non-affine regime and the data below jamming, i.e. $|\gamma| \geq 1$, where the data start to deviate from the power law scalings, Eq. (2).

2-2. Conditional probability distributions (CPDs)

Figure 3 shows the CPDs multiplied by $|\gamma|$, where we introduced $\Xi_n \equiv \xi' - f_n(\xi)$ ($n = c$ and v). Here, the CPDs for both compression ($\gamma > 0$) and decompression ($\gamma < 0$) are well fitted by the Gaussian, stable distribution, and exponential distributions, in (CC), (VV), (CV), and (VC), respectively.

Figure 4 shows the CPDs in (CV) and (VC) for both compression and decompression, where their ξ-dependences are well described by the cumulative distributions of the CPDs in (CC) and (VV), i.e. $1 - I_{CC}(\xi)$ and $1 - I_{VV}(\xi)$, respectively.

Therefore, the CPDs depend only on the magnitude, $|\gamma|$, but do not change their shapes by the sign of γ, i.e. compression or decompression.

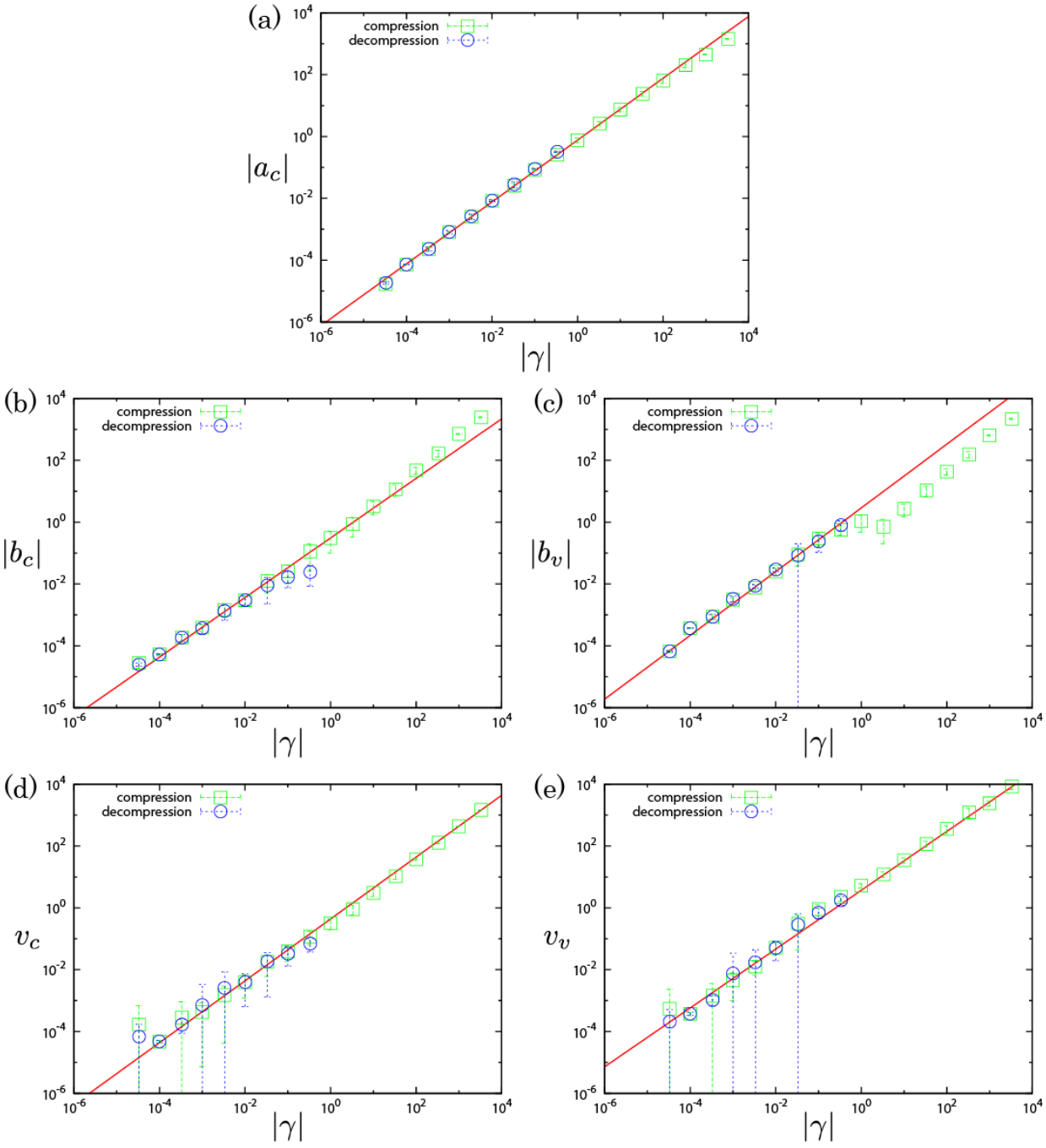

Figure 2. Double logarithmic plots of (a) the slopes in (CC), a_c, (b) offsets in (CC), b_c, (c) offsets in (VV), b_v, (d) fluctuations in (CC), v_c, and (e) fluctuations in (VV), v_v, where the open squares and circles represent compression and decompression, respectively. The solid lines are the power law fitting functions, Eq. (2), for $|\gamma| < 1$. The slopes and offsets, a_c, b_c, and b_v, are negative for decompression, $\gamma < 0$.

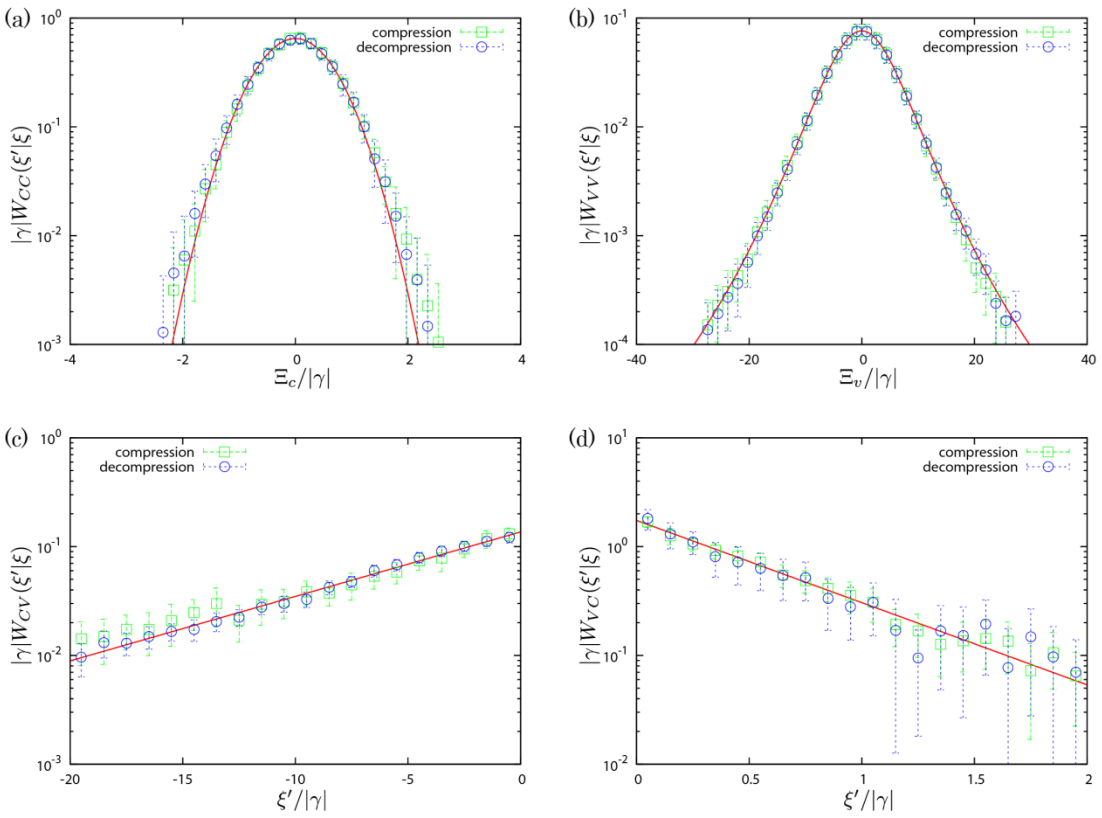

Figure 3. Semi-logarithmic plots of the CPDs in (a) (CC), (b) (VV), (c) (CV), and (d) (VC), where the open squares and circles represent compression and decompression, respectively. The solid lines are the distribution functions, Eqs. (4)-(7), in the manuscript. Here, we fix ξ = (a) 1.2, (c) 0.2, and (d) -0.2, respectively, while we averaged the CPDs in (VV) over the range, $-20 \leq \xi \leq 0$. The scaling parameters are given by $|\gamma|$ = (a) 10^{-3}, (b) 3×10^{-4}, (c) 0.1, and (d) 0.1, respectively.

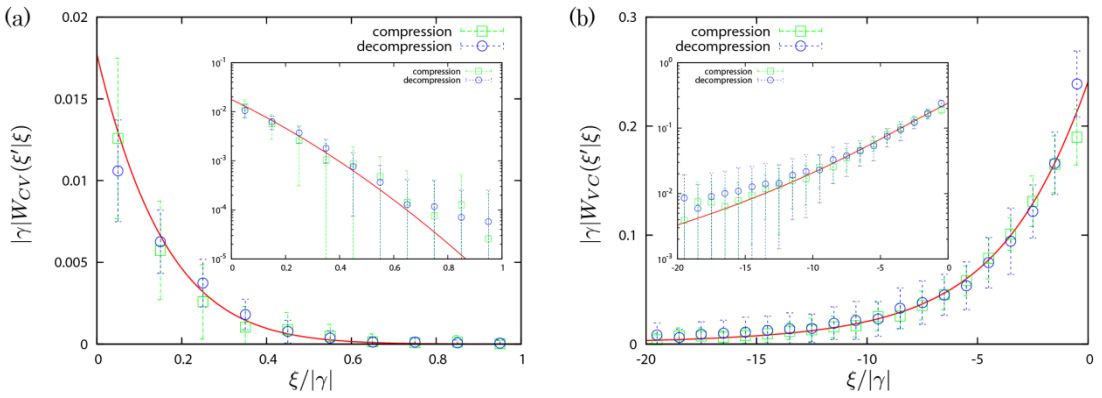

Figure 4. The CPDs in (a) (CV) and (b) (VC) plotted against $\xi/|\gamma|$, where the open squares and circles represent compression and decompression, respectively. The solid lines are the distribution functions, Eqs. (6) and (7), in the manuscript. Here, we fix ξ' = (a) -0.2 and (b) 0.2, respectively, and the scaling parameter is $|\gamma| = 0.1$. The insets are semi-logarithmic plots.

3. The Master equation

In this section, we show an unfolded form of the Master equation. Because the CPDs are separately defined in (CC), (VV), (CV), and (VC), the transition rates in the Master equation are also divided into the four regions as $T_{CC}(\xi'|\xi) \equiv \lim_{\delta\gamma\to 0} W_{CC}(\xi'|\xi)/\delta\gamma$, etc. Then, the Master equations for the PDFs of positive ($\xi' > 0$) and negative ($\xi' < 0$) overlaps are given by

$$\frac{\partial}{\partial\gamma}P_\phi(\xi') = \begin{cases} \int_0^\infty \left[T_{CC}(\xi'|\xi)P_\phi(\xi) - T_{CC}(\xi|\xi')P_\phi(\xi')\right]d\xi + \int_{-\infty}^0 \left[T_{VC}(\xi'|\xi)P_\phi(\xi) - T_{CV}(\xi|\xi')P_\phi(\xi')\right]d\xi, \\ \int_{-\infty}^0 \left[T_{VV}(\xi'|\xi)P_\phi(\xi) - T_{VV}(\xi|\xi')P_\phi(\xi')\right]d\xi + \int_0^\infty \left[T_{CV}(\xi'|\xi)P_\phi(\xi) - T_{VC}(\xi|\xi')P_\phi(\xi')\right]d\xi, \end{cases}$$

respectively, where the second terms in the right-hand-sides represent the gain and loss of contacts due to closing and opening contacts.

Solutions of the Master equation is independent of initial conditions. Figures 5 and 6 display numerical solutions of the Master equations with different initial conditions, where we find that the solutions converge to the same function after several compression steps. Note that the Master equation generates a "gap" around zero, even though the initial condition is continuous at the zero-overlap (Fig. 6).

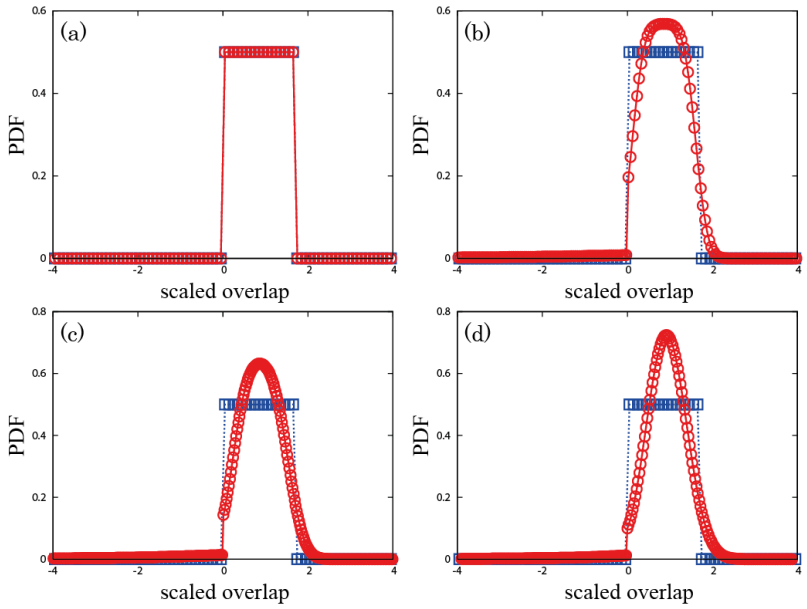

Figure 5. Numerical solutions of the Master equation under compression (red open circles), which develop from (a) to (d), where the initial condition is given by a step function (blue open squares).

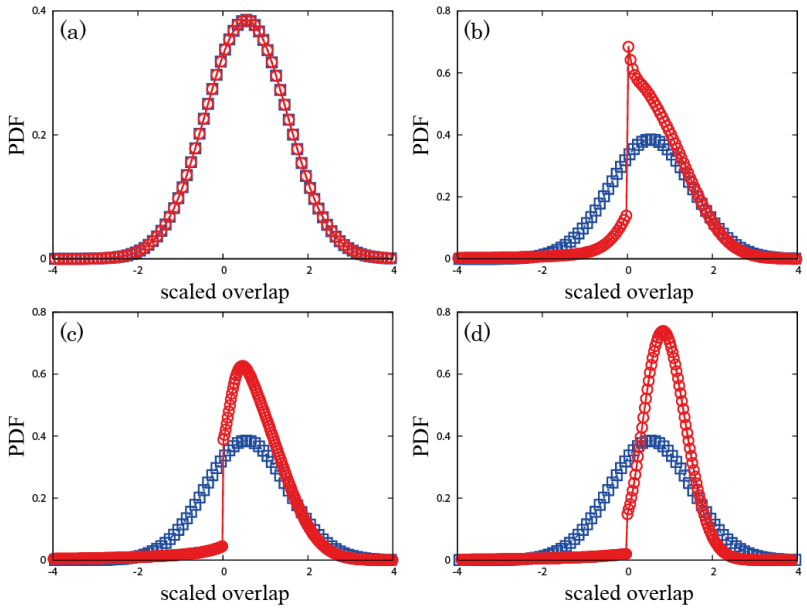

Figure 6. Numerical solutions of the Master equation under compression (red open circles), which develop from (a) to (d), where the initial condition is given by a Gaussian distribution function (blue open squares).

Next, we explain the mechanism for generating "gaps" in the PDFs. Here, we note that the different dimensionless length scales in the CPDs in (CV) and (VC), $q_c \ll q_v$, are important for generating the gaps.

Figure 7 shows (a) affine and (b) non-affine changes of the PDFs under compression. For simplicity, we consider an ordinary Gaussian PDF, because it has no gap before compression and after affine deformation. As shown in Fig. 7(a), the affine deformation shifts the initial PDF to positive overlaps, where the shaded area corresponds to the amount of new contacts. However, the repulsive forces between soft particles push the new contacts back so that the typical "penetration" is reduced to the dimensionless length, $q_c \approx 0.65$, in the exponential distribution in (VC), which is considerably smaller than the maximum penetration by affine deformation, $B_v \approx 1.8$, i.e. three times smaller. Then, the overlaps between new contacts decrease as shown by the short arrows in Fig. 7(b) and the PDF near the zero-overlap (in positive side) grows. At the same time, some (existing or generated) contacts open to virtual ones. Once soft particles are detached from each other, the new virtual contacts can increase freely, because there is no force between these particles. The typical magnitude of generated negative overlaps is represented by $q_v \approx 6.10$ in the exponential distribution in (CV), which is much larger than q_c, i.e. ten times larger. Then, the new virtual contacts widely distribute in negative overlaps, as indicated by the long arrow in Fig. 7(b), so that the PDF near the zero-overlap (in negative side) becomes smaller than that in positive side. As a result, a gap between positive and negative sides is generated.

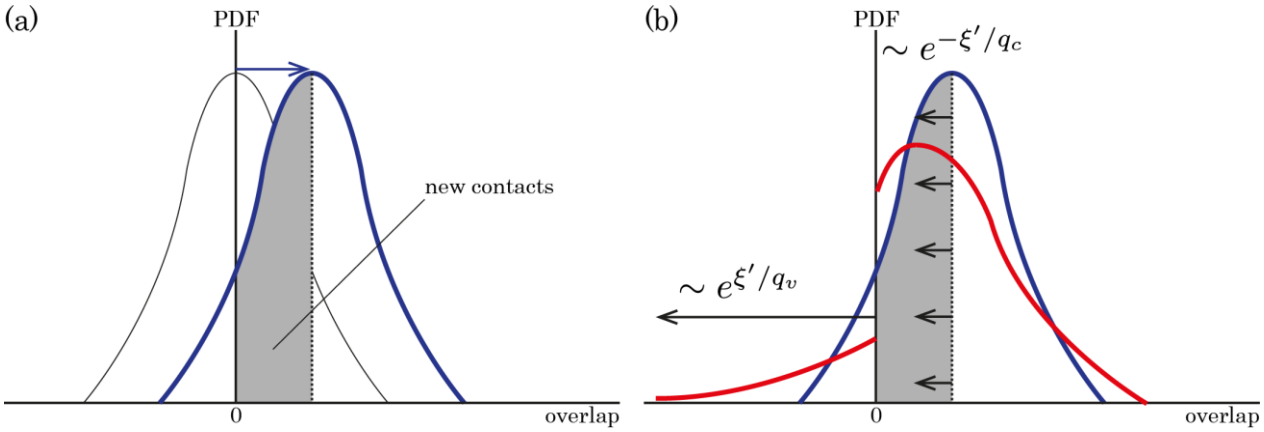

Figure 7. (a) Affine and (b) non-affine changes of a PDF. (a) The initial Gaussian PDF (thin solid line) shifts to the PDF after affine deformation (blue solid line), where the shaded area corresponds to the amount of new contacts. (b) The PDF after affine deformation (blue solid line) changes to the PDF (red solid line) due to non-affine deformations, where typical "penetration" lengths of new contacts and virtual contacts are given by q_c and q_v, respectively ($q_c \ll q_v$).

4. Applications

In this section, we show some applications of the Master equation. At first, we introduce the n-th moment of "positive" overlaps as

$$M_n \equiv \int_0^\infty x^n P(x)dx = \int_0^\infty x^n P(\xi)d\xi \ , \qquad (3)$$

where x is unscaled positive overlaps and we used the relation, $P(x)dx = P(\xi)d\xi$. Then, the coordination number, averaged positive overlap, and elastic energy density are proportional to the 0th, 1st, and 2nd moments, i.e. $z \propto M_0$, $\bar{x} \propto M_1$, and $e \propto M_2$, respectively. The hydrostatic pressure and bulk modulus can be deduced from the first and second derivatives of the energy density, e, against applied strain, where the derivatives are given by the Master equation.